Adaptive Estimation of Complex Calibration Residual Errors of Wafer-Level S-Parameters Measurement System

Aleksandr A. Savin[1)], Vladimir G. Guba[2)], Andrej Rumiantsev[3)], Benjamin D. Maxson[4)], Dirk Schubert[5)] and Uwe Arz[5)]

[1)]*Tomsk State University of Control Systems and Radioelectronics, 634050, Tomsk, Russia*
[2)]*NPK TAIR, a subsidiary of Copper Mountain Technologies, 634041, Tomsk, Russia*
[3)]*MPI Corporation, Advanced Semiconductor Test Division, 30267, Chu-Pei City, Taiwan*
[4)]*Copper Mountain Technologies, 46268, Indianapolis, USA*
[5)]*Physikalisch-Technische Bundesanstalt (PTB), 38116, Braunschweig, Germany*

Abstract — This article presents a method for determining complex residual errors of calibrated two-port vector network analyzers. It utilizes the time-domain technique. Calibration residual errors are extracted from a distance-frequency system model using a special estimation algorithm based on the quasi-optimal unscented Kalman filter. Because the method requires only three measurement conditions, it is in particular beneficial for on-wafer applications, as three test conditions can be obtained from using only one transmission line. Moreover, the length of the line can be relatively short. Experimental studies were performed and verified the proposed method.

Index Terms — S-parameters, vector network analyzer (VNA), verification, residual errors, on-wafer measurements, unscented Kalman filter (UKF).

I. Introduction

The estimation of the vector network analyzer (VNA) calibration residual errors is a crucial step in establishing *S*-parameter measurement assurance. An analysis of different methods was made and the new method of measuring complex calibration residual errors was introduced in [1]. The method required six measurement conditions obtained from reference standards (such as a transmission line and two offset reflection elements) with fully-known electrical characteristics. It was verified for coaxial and wafer-level applications. To increase the estimation accuracy at the wafer-level, the reflection verification elements should be realized as long lines terminated with a short at one end. As a consequence, the verification chip takes undesirably large space of the wafer real estate making the implementation of the proposed method less practical.

This work introduces an adaptive algorithm that allows using reference reflection elements with only partly-known reflection coefficients. As a result, estimation of the calibration residual errors of a wafer-level measurement system can be completed using only one verification element, such as a long transmission line with known characteristic impedance Z_0 and propagation constant γ. The measurement sequence can be completed as follows. First, the RF probe connected to the VNA port 1 contacts the verification line, and the reflection coefficient of the line opened at its second end is measured (this condition is often called an "open stub"). Next, the RF probe connected to the second VNA port contacts the verification line at its second end and four S-parameters of the line are measured. Last, the first RF probe is elevated in the air and the reflection coefficient of the line is measured using the second RF probe. An accurate model of the open stub measurement condition is not required.

II. System Error Model and Observed Signals

The calibrated *S*-parameter measurement system can be described as shown in Fig. 1, where D_i, T_i, M_i and R_i are calibration residual errors at port i of the VNA (i=1, 2).

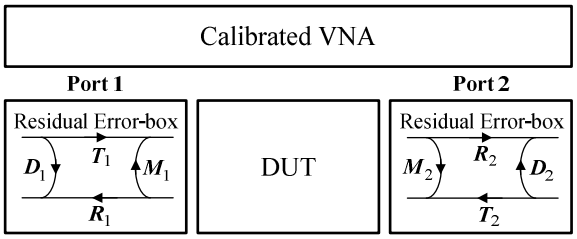

Fig. 1. The model of a two-port calibrated measurement system.

We describe the calibration residual error model of the VNA in the time domain as a set of ten networks, so-called "reflectors". Each reflector has known distance (time delay) and unknown frequency characteristics. For example, Fig. 2 shows the set of samples for A (reference values A_1, A_2, A_3) and B (reference values B_1, B_2, B_3) reflectors in the distance-frequency plane.

In Fig. 2, f_1 is the start frequency, while f_2 and f_3 are other reference frequencies, Δf is the frequency step between samples, l_A is the distance of A from the reference plane of VNA, l_B is the distance of B, and Δl is the distance step between reflectors depending on the length of the on-wafer transmission line. Cubic splines are used to interpolate the frequency characteristics of the reflectors and to calculate A_k and B_k.

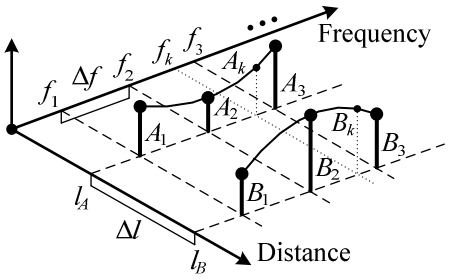

Fig. 2. Distance-frequency model of the measurement system.

The first (reflection) measurement condition gives:

$$\Gamma_1 \approx D_1 + T_1R_1 \cdot (L^2 \cdot G) + M_1 \cdot T_1R_1 \cdot (L^2 \cdot G)^2 , \qquad (1)$$

where L – the transmission coefficient of the line; G – the reflection coefficient at the second (opened) end of the line. L and G can be written as: $L = L_C \cdot \Delta L$ and $G = G_C \cdot \Delta G$, where L_C and G_C are calculated (approximated) parameters, ΔL and ΔG are approximation uncertainties. Thus, (1) includes three unknown reflectors D_1, $T_1R_1 \cdot (\Delta L^2 \cdot \Delta G)$ and $M_1 \cdot T_1R_1 \cdot (\Delta L^2 \cdot \Delta G)^2$ separated from each other in the time domain.

The second measurement condition gives:

$$S_{11} \approx D_1 + M_2 \cdot T_1R_1 \cdot L^2 . \qquad (2)$$

$$S_{21} \approx T_1R_2 \cdot L . \qquad (3)$$

where S_{11} and S_{21} are the measured reflection and transmission coefficients of the verification line, respectively. Thus, (2) and (3) include two new unknown reflectors $M_2 \cdot T_1R_1 \cdot \Delta L^2$ and $T_1R_2 \cdot \Delta L$.

The equations for the second residual error box are obtained in a similar way from the reverse direction of the second measurement condition and the third measurement condition.

III. Algorithm

The algorithm for estimating the frequency characteristics of reflectors was developed using the Markov theory of nonlinear filtering. The algorithm is based on the unscented transformation, and is also known as Unscented Kalman Filter (UKF) [1, 2]. Thus, ten reflectors are calculated using this special time-domain filtering technique:

$$x_1 = D_1 ; \; x_2 = T_1R_1 \cdot (\Delta L^2 \cdot \Delta G) ; \; x_3 = M_1 \cdot T_1R_1 \cdot (\Delta L^2 \cdot \Delta G)^2 ;$$

$$x_4 = M_2 \cdot T_1R_1 \cdot \Delta L^2 \; ; \; x_5 = T_1R_2 \cdot \Delta L ;$$

$$x_6 = D_2 ; \; x_7 = T_2R_2 \cdot (\Delta L^2 \cdot \Delta G) \; ; \; x_8 = M_2 \cdot T_2R_2 \cdot (\Delta L^2 \cdot \Delta G)^2 ;$$

$$x_9 = M_1 \cdot T_2R_2 \cdot \Delta L^2 \; ; \; x_{10} = T_2R_1 \cdot \Delta L .$$

Estimates x_1 and x_6 give the effective directivity of the VNA ports. Estimates x_5 and x_{10} define the transmission tracking with the accuracy factor ΔL. Combining estimates, one can find:

$$\Delta L \cdot \Delta G = \sqrt{\frac{x_2 \cdot x_7}{x_5 \cdot x_{10}}} . \qquad (4)$$

Assuming that both ΔL and ΔG are close to 1, the root-square problem of (4) can be solved. Combining x_2, x_7 and (4):

$$T_1R_1 \cdot \Delta L = x_2 / (\Delta L \cdot \Delta G) , \qquad (5)$$

$$T_2R_2 \cdot \Delta L = x_7 / (\Delta L \cdot \Delta G) . \qquad (6)$$

Therefore, all four residual tracking parameters are found up to the factor ΔL. Next, M_1 and M_2 can be found from x_4, x_9:

$$M_2 \approx M_2 \cdot \Delta L = \frac{x_4}{x_2} \cdot (\Delta L \cdot \Delta G) , \qquad (7)$$

$$M_1 \approx M_1 \cdot \Delta L = \frac{x_9}{x_7} \cdot (\Delta L \cdot \Delta G) . \qquad (8)$$

IV. Experimental Results and Discussion

The goal of the experiments was to verify the proposed method when a verification line has relatively short length, and to evaluate the approximation uncertainties ΔL, ΔG. We used the GaAs Reference Material RM8130 and the multiline TRL method from NIST for calibration of the experimental setup [3, 4]. RM8130 includes five lines in a coplanar waveguide design from which we selected the 19.7 mm (L19) and 6.562 mm (L6) long lines as verification elements. All line lengths are indicated as additional lengths relative to 0.5 mm long thru standard.

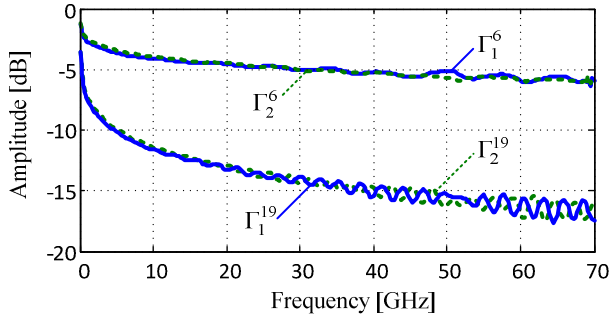

Fig. 3. The measured reflection coefficients of the verification lines open stub conditions corrected by the first calibration series.

All the systematic errors of the measurement setup were calculated from the same set of measured data. Three calibration conditions were investigated: first series – using all available lines, second series – using all available lines except line L6, and third series – using all available lines except line L19. The first (complete) calibration series provided the reference data, as this calibration is expected to be the most accurate. Measurement frequencies covered the band from 100 MHz to 70 GHz with 286 frequency steps. Figures 3-6 show the verification measurements using L6 and L19 as verification lines in the frequency and in the time domain,

respectively. Residual errors and their products can be well identified in the time domain diagrams (Fig. 5, 6).

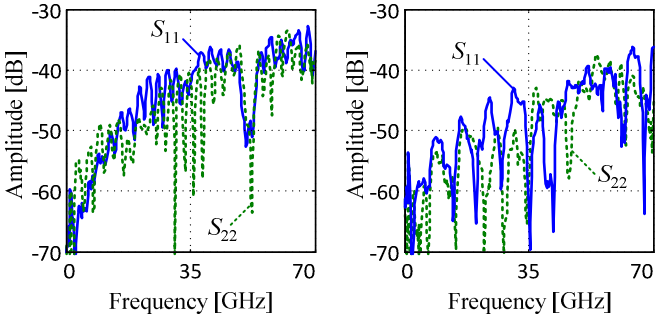

Fig. 4. The measured reflection coefficients of L19 (left) and L6 (right), first calibration series.

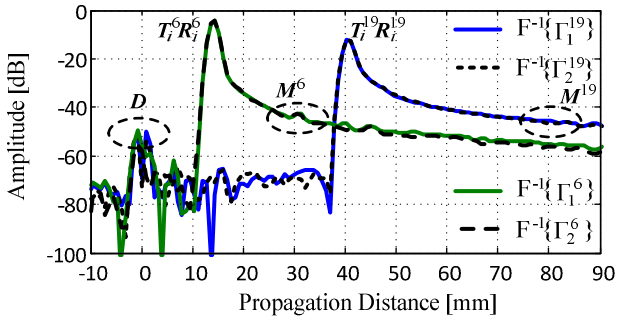

Fig. 5. Reflection time domain diagrams of the open stub conditions for the two verification lines L19 and L6.

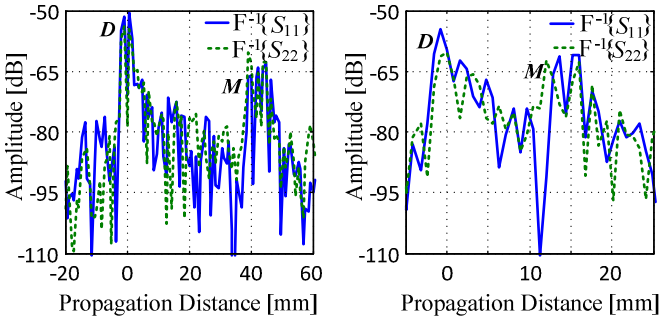

Fig. 6. Reflection time domain diagram of S_{11} and S_{22} of the verification lines L19 (left) and L6 (right).

Next, the calibration residual error terms of the test system were calculated. The minimal frequency step Δf for calculated reference points depends on the length of the verification line and is Δf_{L19}=2.8 GHz for L19 and Δf_{L6}=8.4 GHz for L6. The use of a short reference line is an obvious practical advantage, however, it may reduce the estimation accuracy, as $\Delta f_{L19}<\Delta f_{L6}$. In Fig. 7 we compare residual errors of the first (reference) calibration series when using L19 as verification line with Δf=2.8 GHz and Δf=8.4 GHz frequency steps. The comparison demonstrates that the choice of Δf=8.4 GHz introduces only negligible calculation errors, except for the residual directivity D_1 at frequencies around f=51 GHz (Fig. 7). The cause of the observed anomalous drop in D_1 is probably specific to our measurement setup.

In the following, further comparisons of L6 and L19 verification results are performed using the same frequency step Δf=8.4 GHz. This may slightly overestimate the residual directivity D_1 in the frequency range from 45 GHz to 55 GHz.

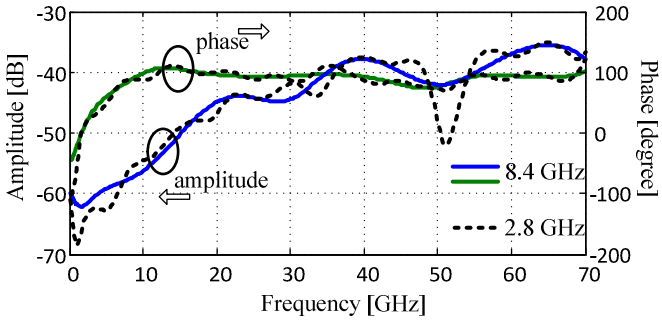

Fig. 7. The magnitude and the phase of the residual error D_1 of the first calibration series estimated using L19 as verification line with Δf=8.4 GHz (solid lines) and Δf=2.8 GHz (dotted lines).

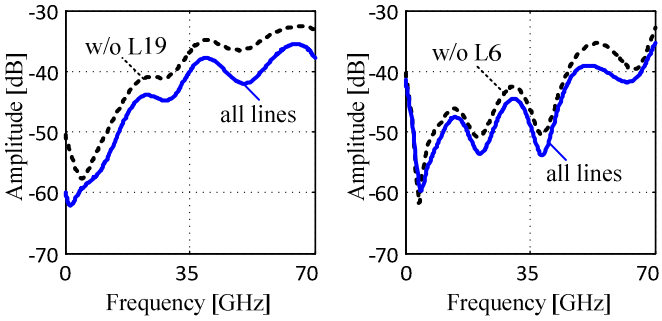

Fig. 8. The magnitude of the residual directivity D_1 using the verification lines L19 (left) and L6 (right) for the three calibration series. Calibration accuracy degrades when fewer lines are involved in the calibration process.

We calculated residual errors of the three calibration series from verification measurement data of both lines L6 and L19. Fig. 8 shows the forward residual directivity D_1, while Fig. 9 shows residual reflection and transmission tracking T_1R_1 and T_1R_2, respectively. Other parameters demonstrated a similar relationship. As expected, the accuracy of the calibration degrades when fewer lines are included in the calibration step. The longest line L19 influences the calibration process the most.

We observed a slight variation of the obtained residual errors for the reference calibration series when L6 and L19 were used for the verification measurement (Fig. 9). The method assumes that the propagation constant of both lines is identical. However, as it was discussed in [5], possible coupling of the verification line with nearby structures through the substrate as well as its interference with the probe tip may lead to the propagation of higher-order modes and thereby to a slight distortion of the propagation constant.

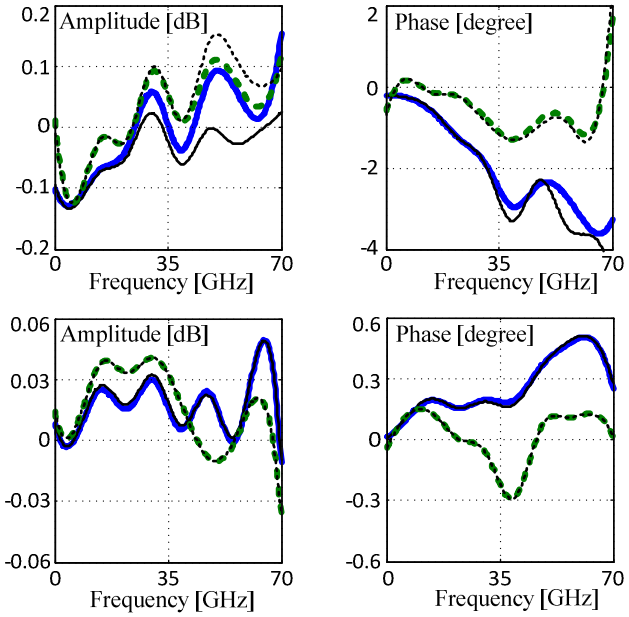

Fig. 9. Comparison of the magnitude and the phase of the residual reflection tracking T_1R_1 (top) and the residual transmission tracking T_1R_2 (bottom) for several verification and calibration cases: 1) L19, first series (solid thick lines); 2) L19, third series (solid thin lines); 3) L6, first series (dotted thick lines); and 4) L6, second series (dotted thin lines).

We also verified our initial assumption about ΔL and ΔG made when solving (4). The magnitude and the phase of the product $\Delta L \Delta G$ are given in Fig. 10. It is important to note that this product is originally unknown, similarly to the reflection coefficient of the reflect standard used for TRL calibrations.

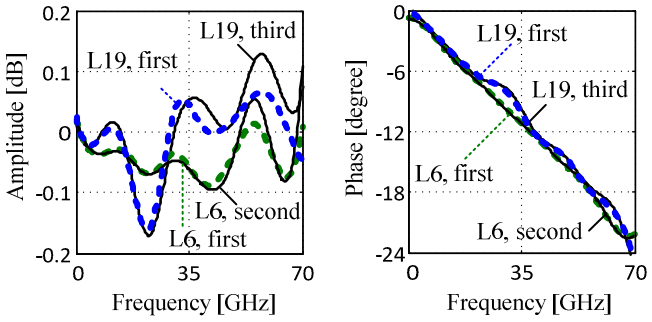

Fig. 10. Magnitude (left) and phase (right) of $\Delta L \Delta G$ as calculated by (4) for L6 and L19 as verification lines (all calibration series).

Often, the calibration reference impedance Z_{REF} and the characteristic impedance Z_0 of the verification line are different. In this case, the calculated calibration residual errors can be easily transformed into the system of the desired reference, in a manner similar to that proposed in [6]. We used the characteristic impedance Z_0 of L6 and L19 extracted from previous experiments (Fig. 11, right) and transformed the results to Z_{REF}=50 Ω. Fig. 11, left shows D_1 obtained from the first measurement series, with L19 as the verification line, before and after impedance transformation. Above 12 GHz, the influence of the impedance transformation on D_1 seems negligible.

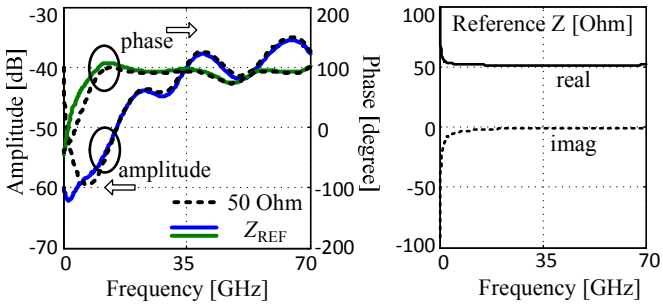

Fig. 11. Comparison of magnitude and phase of the residual directivity D_1 (left) before (solid lines) and after (dotted lines) impedance transformation (first calibration series, L19).

V. Conclusion

In this paper we presented an algorithm for estimation of complex residual errors of a calibrated two-port VNA requiring only one transmission line. The algorithm significantly reduces both the measurement time and the cost of the verification procedure. Experimental results demonstrated suitability of the new method for wafer-level applications.

Acknowledgement

The authors thank Sergey Zaostrovnykh and Alex Goloschokin from Copper Mountain Technologies, Indiana, USA for support of this work and for their helpful discussions.

The work was supported by Russian Foundation for Basic Research RFBR Project 14-07-31312.

References

[1] A. A. Savin, V. G. Guba, A. Rumiantsev, and B. D. Maxson, "Estimation of Complex Residual Errors of Calibrated Two-Port Vector Network Analyzer," *83rd ARFTG Microwave Measurement Conference*, 2014, Tampa, Florida, USA.

[2] A. A. Savin, "A Novel Factor Verification Technique for One-Port Vector Network Analyzer," *Proceedings of the 43rd European Microwave Conference*, 7-10 October 2013, Nuremberg, Germany, pp. 60-63.

[3] "Reference Material 8130. Coplanar waveguide calibration set," NIST, Gaithersburg, MD 20899, USA, 1998.

[4] R. B. Marks, "A multi-line method of network analyzer calibration," *IEEE Trans. Microwave Theory Tech.*, vol. 39, no. 7, pp. 1205-1215, January 1991.

[5] A. Rumiantsev and R Doerner, "Method for estimating probe-dependent residual errors of wafer-level TRL calibration," *83rd ARFTG Microwave Measurement Conference*, 2014, Tampa, Florida, USA.

[6] R. B. Marks and D. F. Williams, "A general waveguide circuit theory," *Journal of research of the National Institute of Standards and Technology*, vol. 97, pp. 533-562, September-October 1992.